Journal of Process Control 88 (2020) 63–77

Contents lists available at ScienceDirect

Journal of Process Control

journal homepage: www.elsevier.com/locate/jprocont

Cloud-based implementation of white-box model predictive control for a GEOTABS office building: A field test demonstration

Ján Drgoňa[a,c,*], Damien Picard[a], Lieve Helsen[a,b]

[a] KU Leuven, Department of Mechanical Engineering, Leuven, Belgium
[b] EnergyVille, Thor Park, Waterschei, Belgium
[c] Pacific Northwest National Laboratory, Richland, WA, USA

ARTICLE INFO

Article history:
Received 4 October 2019
Revised 8 January 2020
Accepted 15 February 2020
Available online 9 March 2020

Keywords:
Model predictive control
Building climate control
White-box modeling
Cloud-based implementation
Field test

ABSTRACT

Model predictive control (MPC) has been proven in simulations and pilot case studies to be a superior control strategy for large buildings. MPC can utilize the weather and occupancy schedule forecasts, together with the system model, to predict the future thermal behavior of the building and minimize the overall energy use and maximize thermal comfort. However, these advantages come with the cost of increased modeling effort, computational demands, communication infrastructure, and commissioning efforts. Thus a typical approach is to, often rapidly, simplify the building modeling and MPC optimization problem while paying a price of not reaching the full performance potential. It has been shown that by employing accurate physics-based models, MPC performance can be notably increased closer to its theoretical performance bound. However, implementation of such high-fidelity MPC in real buildings remains a challenge, resulting in a lack of successful field test studies. This work presents the methodology and field test demonstration of a computationally efficient implementation of the white-box MPC in an office building in Belgium. The detailed model of the building is based on first-principle physical equations. The deployment and supervision of MPC operation in a practical setting are supported by an automated cloud-based communication infrastructure. The motivating factor behind the cloud-based architecture is its compatibility with a commercially appealing control as a service concept. The building is equipped with a ground source heat pump (GSHP) and thermally activated building structures (TABS), where the combination of both is also known as GEOTABS. From a control perspective, GEOTABS buildings are particularly challenging systems due to large scale, complex heating, ventilation and air conditioning (HVAC) system, and slow dynamics with time delays. On the other hand, there is an increased potential for energy savings due to the high thermal mass, which acts as thermal storage. The MPC operation is demonstrated during the challenging transient seasons (switching between heating and cooling), and its performance is compared to a traditional rule-based controller (RBC). We provide a proof of concept of real MPC operation for the most difficult seasons with notable GSHP energy use savings equal to 53.5% and thermal comfort improvement by 36.9%. Other MPC applications found in the literature describe tests for only cooling or only heating, and up to now only for a black-box or a grey-box approach.

1. Introduction

Nowadays buildings use roughly 40% of the global energy (approx. 64 PWh), a large portion of which is being used for heating, cooling, ventilation, and air-conditioning (HVAC) [1]. The energy efficiency of buildings is thus a priority to sustainably address the increased energy demands and reduction of CO_2 emissions in the long term. Recently revised EU policy on the energy performance of buildings states that large buildings should be equipped with building automation and control systems by 2025 if economically and technically feasible [2]. Despite these trends manually tuned rule-based control (RBC) strategies remain business as usual in the building industry [3].

However, this situation is far from ideal. Poorly tuned RBC often causes thermal comfort problems, such as overheating, undercooling, imbalance in zone temperatures, or fluctuating and fast tem-

* Corresponding author.
E-mail addresses: jan.drgona@kuleuven.be (J. Drgoňa), damien.picard@kuleuven.be (D. Picard), lieve.helsen@kuleuven.be (L. Helsen).

https://doi.org/10.1016/j.jprocont.2020.02.007

perature changes. The control performance of RBC is often dropping with increased complexity and time constants of the controlled building due to challenging manual tuning of RBC. Modern large scale office buildings are often equipped with production systems in a hybrid configuration, combining energy-efficient production units (e.g., heat pump (HP)) with less energy efficient supplementary systems (e.g., gas boilers (GB)). The complexity also rises with multiple emission systems with different time constants, for example, slow thermally activated building structures (TABS) or floor heating (FH), and fast fan coil units (FCU) or radiators. Specifically challenging cases are geothermal thermally activated building systems with two or more production systems, also called hybrid GEOTABS buildings [4]. On top of that, the stochastic nature of the weather and occupancy patterns have the potential to deteriorate the performance of any manually tuned control strategy with a set of fixed rules.

It has been proven that smart control strategies, like model predictive control (MPC) can significantly mitigate emissions of greenhouse gases, improve the thermal comfort of the occupants while simultaneously reducing the energy use, with average savings of 15% up to 50% [5–9]. Unfortunately, the transition of this technology to practice is slow. This is partially due to the conservative building sector, but the main reason is that the implementation, commissioning, and maintenance of MPC in practice remain a real challenge [10,11]. There are several causes of this situation. First, every building is a unique system which requires tailored modeling and control design. However, building control engineers do not have advanced education in modern energy modeling and optimal control methods and tools. Additionally, MPC demands elaborate ICT infrastructure with decent sensor accuracy, which is often not the case in contemporary buildings. Even if the building is well equipped, the lack of standardization and closed software solutions of commercial building management system (BMS) vendors imposes increased engineering time and cost for the development of an advanced control strategy.

Due to these difficulties, most of the demonstrations of MPC in real buildings are using considerable simplifications of the underlying building models. One of the first applications of MPC for control of the building of the Czech Technical University in Prague were reported in [7,12]. A gray-box model identified from the measurement data was used to predict the building's thermal response. Measured energy savings during the heating season spanned between 15 and 28%, depending on various parameters, mainly insulation level and outside temperature. Another pilot case study with MPC for building cooling systems equipped with thermal energy storage at UC, Merced campus, USA reported an improvement of 19% in the coefficient of performance (COP) compared to the original baseline logic [13]. An application of MPC with an economic objective for optimizing the building energy cost was used to demonstrate peak shaving capabilities for energy demand-side management [14]. Agent-based MPC saved around 8% of operational cost for the heating and cooling system in an office building in Ottawa [15]. Another case study using a gray-box prediction model obtained more than 30% energy saving during the winter in an office building in Brussels, Belgium [16]. A recent implementation with a four-month experimental test period shows a 29% HVAC electric energy reduction and a 63% thermal energy reduction compared to previous years for the same time period by using MPC [17]. A similar approach to that presented in this paper describing a proposal for the practical implementation of the white-box MPC for an office building without operational data can be found in [18]. Recently, data-driven MPC solutions have also been successfully applied to improve the cooling energy efficiency for the data centers [19,20]. From a theoretical and technological perspective, the HVAC control for data centers is practically identical to the control of modern office buildings. Therefore the white-box MPC approach presented in this paper is by no means limited to the office buildings and could also represent a viable candidate for the data centers cooling applications.

The building used in this work (called Hollandsch Huys) is located in Hasselt, Belgium and was previously used for assesment of building thermal models and predictive controllers. The development of the methodology for gray-box system identification targeted to MPC was reported in [11]. Despite the poor quality of measurement data obtained from BMS, the model was able to make two days ahead predictions with a mean error of approximately 0.3 °C. In 2014, the identified 8th order gray-box model was used by MPC operating two weeks during the heating season with 17% energy savings [21]. A later simulation case study using a detailed emulator model compared MPC performance with different controller models reported that the white-box MPC outperformed gray-box MPC in terms of energy savings by 50% [22]. This finding is supported by unrelated simulation case study reporting that the MPC performance for buildings is sensitive to the prediction accuracy of the controller model, highlighting the potential performance improvement obtained by more accurate higher-order physical models [23].

In this paper, we present the methodology, successful cloud-based implementation, and field test demonstration of the white-box MPC in a GEOTABS office building in Hasselt, Belgium. We provide a description of the validated high fidelity building model characterized by more than 700 state variables, 300 disturbance signals, 12 thermal zones and 21 control inputs projected onto 35 actuator variables. In comparison with the simplified gray-box approach [21], the main added value of the detailed physical-based modeling is its accuracy, reliability, and interpretability. All state variables have a physical meaning and can be spatially located within the building structure. Additional added value is the use of an automated cloud-based communication infrastructure with a user-friendly web-based interface, which simplifies the development and supervision of MPC operation in a practical setting. The viability of the presented white-box MPC approach is demonstrated on a real operation in a fully occupied building during the transient seasons (intermediate between spring to summer, and summer to autumn).

The centralized hierarchical control configuration consists of MPC and state estimation on a higher level and heuristic rules together with P/PI controllers on a lower level. We show how to keep the computational time of the corresponding optimal control problem (OCP) tractable even for a large scale system with long prediction horizon. We achieve this by decoupling the input and disturbance non-linearities from the linearized building envelope dynamics. Non-linear disturbances are pre-computed using a non-linear simulation model parallel to linear MPC. Non-linearities in control inputs are decoupled via post-processing by solving a separate but smaller non-linear optimization problem. We present a reliable real-time execution procedure with error handling functionality as an indispensable part of any real implementation, ensuring a robust operation even in the presence of computer shutdowns or communication errors. Moreover, a standardized notation for MPC formulation in the building control domain is used to facilitate the information exchange between mechanical and control engineering communities as a preliminary result of joint effort within IBPSA Project 1.[1]

The paper is organized as follows. Section 2 presents the building investigated together with the white-box based modeling approach. The standardized notation, control configuration with

[1] https://ibpsa.github.io/project1/.

(a) Building from outside.

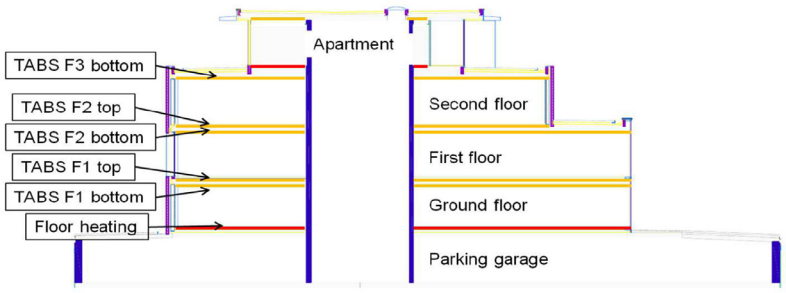

(b) Building's layout.

Fig. 1. Hollandsch Huys office building [24].

state estimation, MPC formulation and non-linear post-processing of control variables are presented in Section 3. Section 4 provides details about cloud-based communication infrastructure and practical aspects of the development and operation of MPC. The demonstration of MPC operation is presented in Section 5. Finally, Section 6 concludes the paper.

2. Office building

This section provides a high-level overview of the building and its systems. This section is based on prior modeling work done by Picard [9]. The case study office building shown in Fig. 1a, called *Hollandsch Huys*, is located in Hasselt, Belgium. Its construction was finished in 2007 and it was designed to be a low-energy, innovative building. Fig. 1b shows the building's layout, which consists of five floors: underground parking, three floors, and a roof apartment. The following sections describe the building envelope, the HVAC system, the control oriented model, the occupancy, internal gains, comfort bounds assumed and RBC.

2.1. Building envelope

The general parameters of the building envelope are summarized in Table 1. The U-value is an average value for the thermal transmittance, representing the rate of transfer of heat through the whole building structure. ACH (n50) stands for *air changes per hour* through the building envelope under a 50 Pa pressure difference. The loss area represents a total heat loss surface of the building envelope. The building is divided into 12 thermal zones, 4 per floor. All transparent parts of the façade are equipped with triple glazing. The window surface lies 40 cm deeper than the façade. Each of them is equipped with an external slat shading device whose angle is adjusted automatically to the solar radiation intensity: the shading device is controlled by a hysteresis controller which closes the shading when the horizontal solar radiation exceeds 150 Wm^{-1} and re-opens it when the solar radiation is lower than 80 Wm^{-1}.

2.2. Heating ventilation and air conditioning system

Fig. 2 shows the hydraulic scheme of the building. Hollandsch Huys represents a so-called *hybrid GEOTABS* building with the emission system composed of a central air handling unit (AHU), floor heating (FH) on the ground floor, and thermally activated building structures (TABS) with a floor and a ceiling circuits on individual floors, see Fig. 1b. The nominal mass flow rates are listed in Table 2. The main production system is a 150kW Daikin EWWP145 KAW1M heat pump (HP) coupled to ground heat exchangers (22 with 75m depth), two buffer tanks of $1m^3$ each, three heat exchangers, and circulation pumps. An additional gas boiler (GB) is installed in the building to back up the heating of the ventilation air but it is not included in the model as it is not needed when proper control is used.

Table 1
General building parameters [9].

Floor area	[m^2]	3760	U-value	[$Wm^{-2}K^{-1}$]	0.216
Conditioned volume	[m^3]	10526	Loss area	[m^2]	4438
Window-to-wall ratio	[-]	34%	ACH (n50)	[h^{-1}]	0.9

2.3. Rule-based controller

Fig. 3 explains the logic of the rule-based controller (RBC) installed in Hollandsch Huys based on three different modes: the heating (H), the passive cooling (PC) and the active cooling (AC) mode. The controller can switch from mode to mode once per hour to avoid fast switches between the modes. The temperature of the storage tanks are controlled using a PI-controller which modulates the heat pump based on the feedback from the measurement of the buffer tank temperature with the set-point given by the heating/cooling curves for the TABS and floor heating (see Fig. 4). The TABS and floor heating circuits are controlled as follows: each hour, the water is circulated in each circuit for 10 minutes. Depending on the difference between its supply temperature and its return temperature, the re-circulation is continued for a given amount of time (see 3). It should be noted that the starting time of the different circuits is shifted by 10 minutes relative to each other in order to smooth the thermal demand loads. A detailed description of RBC can be found in [9].

2.4. Control oriented building model

A detailed white-box non-linear building model was developed in [9] using the Modelica `IDEAS` model library [25]. This model

Table 2
Nominal mass flow rates for TABS and floor heating.

Emission	Nominal mass flow rate			
TABS-ceiling	7	[l h^{-1} m^{-2}]	0.0019	[kg s^{-1} m^{-2}]
TABS-floor	6	[l h^{-1} m^{-2}]	0.0017	[kg s^{-1} m^{-2}]
Floor heating	4	[l h^{-1} m^{-2}]	0.0011	[kg s^{-1} m^{-2}]
Entire building	47,600	[l h^{-1}]	13.22	[kg s^{-1}]

Table 3
Re-circulation times for TABS and floor heating as a function of the difference between the supply temperature $T_{sup}^{TABS/FH}$ and the return temperature $T_{ret}^{TABS/FH}$ [9].

$T_{sup}^{TABS/FH} - T_{ret}^{TABS/FH}$	[K]	3	5	7	9	9+
Extra re-circulation time	[s]	0	600	1200	2000	3000

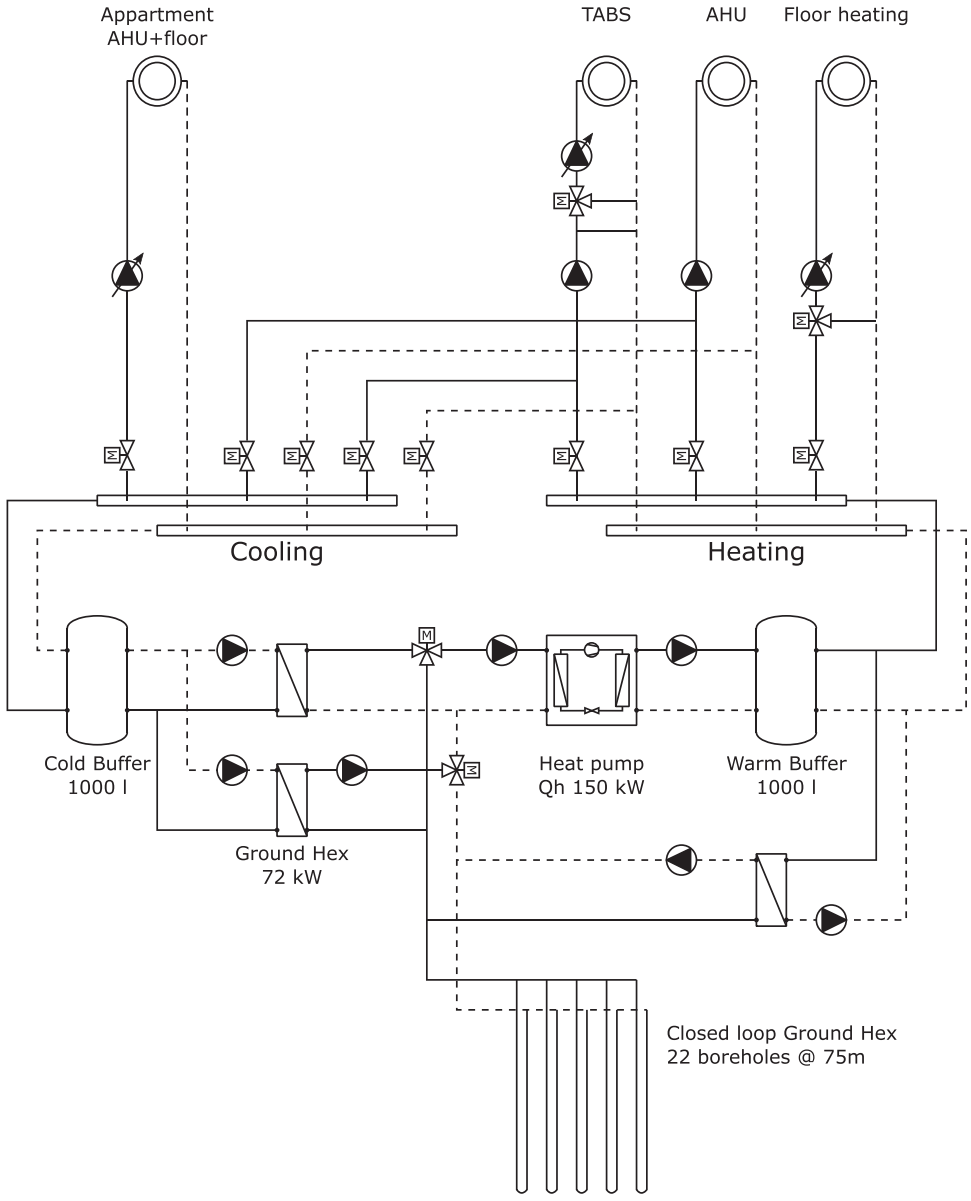

Fig. 2. Hollandsch Huys hydraulic scheme. The components are: borefield, heat exchangers, buffers, heat pump, TABS, floor heating, and 12 circulation pumps.

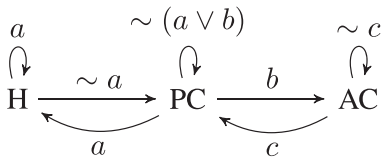

$$a = T_{\text{e3d}} < 12°C$$

$$b = (T_{\text{e}} > 30°C) \wedge \left(T_{\text{top}}^{\text{C,storage}} > T_{\text{sp}}^{\text{C,storage}} + 10°C\right)$$

$$c = \left(T_{\text{top}}^{\text{C,storage}} < T_{\text{sp}}^{\text{C,storage}}\right) \vee (T_{\text{e3d}} < 30°C)$$

Fig. 3. RBC mode selection between the heating (H), the passive cooling (PC) and the active cooling (AC) mode. T_{e} and T_{e3d} are the ambient temperature and its 3-day average, respectively. $T_{\text{top}}^{\text{C,storage}}$ is the temperature in the highest layer of the cold storage tank and $T_{\text{sp}}^{\text{C,storage}}$ its set-point. $\vee$ is the logical conjunction (and), $\wedge$ the logical disjunction (or), and ~ the negation (not) [9].

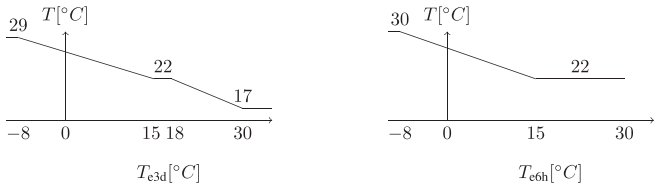

(a) Heating/cooling curve for TABS. *(b) Heating/cooling curve for floor heating.*

Fig. 4. Heating/cooling curves for the supply water to the TABS (a) and to the floor heating system (b) as a function of respectively the previous three days (3d) and previous 6 hours (6h) average ambient temperature (T_{e}).

represents a high-fidelity building emulator, however, due to its complexity, its direct use for control purposes is tedious. Fortunately, the nature of the building's dynamics allows us to use several assumptions to decrease the complexity of the non-linear model in Modelica. First, the building envelope model can be accurately linearized around a working point in order to obtain a lin-

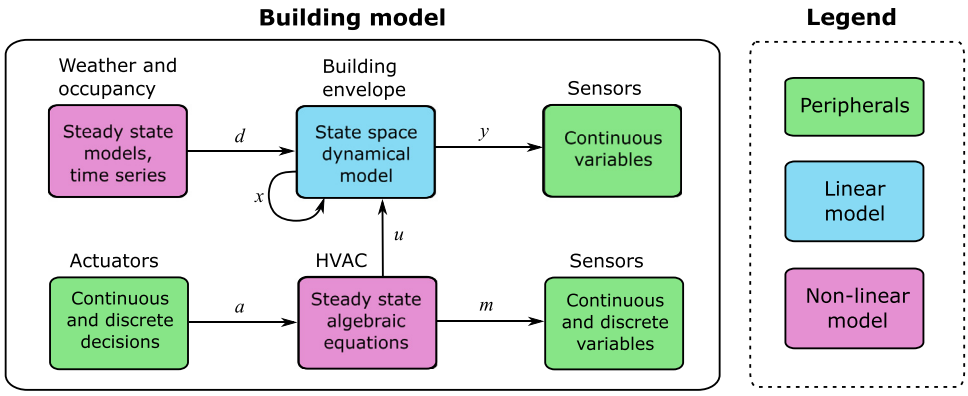

Fig. 5. Structure of the building model with decoupled non-linearities inspired by [18].

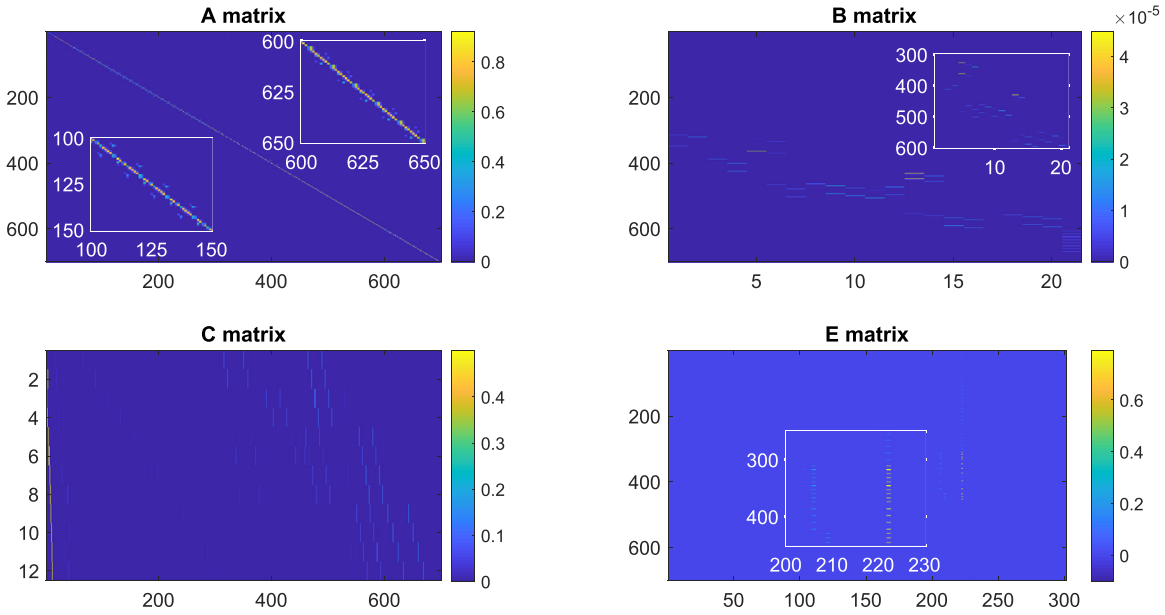

Fig. 6. Heat maps of the linear controller model matrices (1).

ear model. Second, the HVAC dynamics and weather disturbances can be decoupled from the linearized building envelope dynamics to form a Hammerstein-Wiener model structure. Fig. 5 illustrates a general building model structure with the decoupling principle.

The equations for the solar transmission and absorption through the windows are highly non-linear and are pre-computed using the non-linear IDEAS model and they are considered as disturbances d in the linearized state space model (SSM). For a complete description of the linearization process, we refer to [26]. The discretized linear time-invariant (LTI) SSM has the following form:

$$x_{k+1} = Ax_k + Bu_k + Ed_k, \tag{1a}$$

$$y_k = Cx_k + Du_k, \tag{1b}$$

where x_k, u_k and d_k are states, inputs and disturbances at the kth time step, respectively. The model is discretized with a sampling period $T_s = 15$ min. The disturbance signals d_k represent the heat absorption and the direct and diffuse solar radiation for each window, the direct, diffuse solar radiation and the ambient temperature per orientation and inclination, the ambient temperature, and the ground temperature. The matrix A is a state transition matrix which represents the spatial thermodynamical relations of the buildings states (floor, walls, roof, and zone temperatures). The matrix B represents the influence of controllable heat flows (TABS and floor heating) on states, the matrix E represents the influence of disturbances (ambient temperature, solar irradiation, internal gains) on states. Matrix C is a mapping of states onto outputs which represent zone operative temperatures, and matrix D describes the influence of inputs on outputs, which for buildings, is usually a zero matrix, as it is also in the case of Hollandsch Huys. Heat maps of the coefficients of the model matrices are provided in Fig. 6. Blue areas represent coefficients with zero or very low dynamical effect, while yellow areas stand for coefficients with a significant effect on model dynamics. Spatial relations of individual variables cause noticeable sparsity patterns in the model. Due to the high dimensionality, a particular model structure is revealed after zooming in the subset of the model matrices shown in white boxes. The overall dimensions of the building envelope model are summarized in Table 4. A complete list of the system variables and parameters used for control design, together with their physical meaning and units are given in Tables 6–8 of Section 3.1, respectively.

2.5. Disturbance forecast

The internal gains are computed by the stochastic behavioral model of Parys et al. [27] integrated within the non-linear Modelica model. Their nominal values are listed in Table 5. The actual

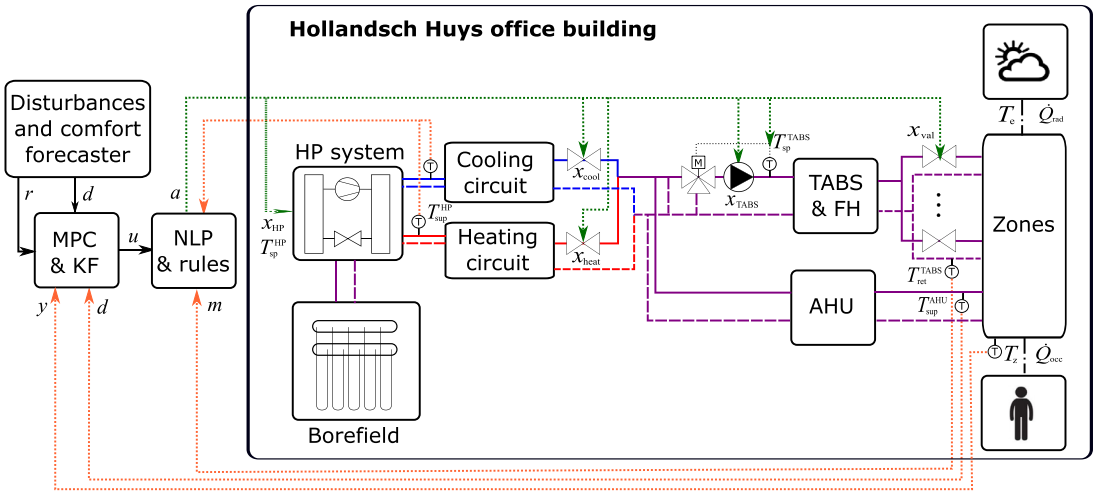

Fig. 7. Model predictive control configuration in Hollandsch Huys. Blue lines represent cooling circuit, red lines represent heating circuit, and purple lines represent main distrubution circuits for both heating and cooling. Full lines stand for supply, and dashed lines stand for return flows. Communication channels are given by dotted lines, green for writing and orange for reading values. Dash dotted lines stand for unmeasured but forecasted disturbance signals, in particular weather and occupancy.

heat gains are obtained by multiplying the nominal values with the stochastic coefficients which are given in [9] Because we are dealing with an office building, the occupancy presence is scheduled between 7:00AM and 8:00PM during the working days.

The weather forecast for Hollandsch Huys is based on real-time weather data from Dark Sky [28]. Data are automatically downloaded using Python Dark Sky API and parsed to the input format for the non-linear Modelica model. For operational purposes, the weather model is extracted from the Dymola environment using the Functional Mockup Interface (FMI). Subsequently, the Dymola FMI kit for Simulink is used as an interface for simulation in the Matlab environment. Here, 20 data points from Dark Sky, stored in a.txt file in TMY format are transformed via an FMI model to 301 disturbance signals d which are used as inputs for the linear model.

2.6. Comfort bounds

Based on the request of the building owner the thermal comfort range is set to 22 °C–24 °C for both heating and cooling season, respectively. The night setbacks are relaxing the comfort abounds by 2 °C. Thermal comfort is kept from 7:00AM to 6:00PM during the week and the ventilation is on from 6:00AM to 8:00PM.

3. Model predictive control

This section describes the design of state estimation, formulation, structure, and technical details of MPC deployment.

3.1. Notation

First, we define the notation for control design, which emerged from the IBPSA Project 1.[2] The used variables are defined in Table 6. We introduce the mapping from the physical domain to the abstract control domain to make the MPC formulation more compact and compliant to the control engineering community standards. The abstract domain variables represent states x, controlled outputs y, other measured variables m, actuator variables a, optimal control actions u, disturbances d, and slack variables s, respectively. The differentiation between u and a is introduced because the computed optimal control actions do not always coincide with physical actuators and an additional post-processing step needs to be performed via mapping $a = f(u)$. The MPC formulation parameters for modifiers and bounds are given in Tables 7 and 8, respectively.

3.2. Control configuration

Fig. 7 shows the corresponding control configuration in Hollandsch Huys after MPC deployment. We choose the centralized configuration where MPC computes the optimal control actions u, based on estimated $\hat{x}$ computed via time-varying Kalman Filter (TVKF). The details of the TVKF implementation can be found in [23]. TVKF uses an augmented state space model to mitigate the plant-model mismatch via offset-free control [29]. Optimal heat flows at the current time step u_0 are subsequently post-processed by a non-linear program (NLP) and heuristic rules to the actuator signals a. The NLP computes the set-points for low-level PID controllers regulating supply temperatures to the TABS and floor heating, as well as the valve modulation signals in individual circuits of the TABS. The HP modulation x_{HP} and activation of the

[2] https://ibpsa.github.io/project1/.

Table 5
Nominal internal heat gains [9].

		People *			Light		Appliances	
Type of room		Convective	Radiative	Latent	Convective	Radiative	Convective	Radiative
Office area	[Wm^{-1}]	1.63	1.63	2.75	3.50	3.50	6.23	8.60
Technical room	[Wm^{-1}]	0	0	0	0	0	0	0

* (assuming 20 m^2 per person as the building is only partially occupied).

circulation pumps x_{TABS} and x_{FH} are selected based on computed heat flows u_0, and supply and return temperatures of TABS and FH. The controlled variables are operative temperatures in 12 thermal zones y. Besides weather and occupancy forecast, the supply temperatures of the AHUs $T_{\text{sup}}^{\text{AHU}}$ are treated as measured disturbance variables d. This decision is a trade-off between complexity and control performance and is motivated by poor tuning of the low-level PID controllers regulating the AHU temperatures, exhibiting overshoots and oscillations during set-point changes. Two possible solutions are re-tuning of the PID controllers within the BMS system or adopting a reference-governor MPC scheme [30]. Both represent the potential for improvement of the control performance in future work.

3.3. Model predictive control formulation

The MPC minimizing energy use and thermal discomfort for the Hollandsch Huys building is given as the following quadratic optimization problem (QP):

$$\min_{u_0,\dots,u_{N_c-1}} \sum_{k=0}^{N-1} ||s_k^{T_z}||_{Q_s}^2 + \sum_{k=0}^{N_c-1} ||u_k||_{Q_u}^2 \tag{2a}$$

$$\text{s.t. } \tilde{x}_{k+1} = \tilde{A}\tilde{x}_k + \tilde{B}u_k + \tilde{E}d_k, \quad k \in \mathbb{N}_0^{N-1} \tag{2b}$$

$$\tilde{y}_k = \tilde{C}\tilde{x}_k + \tilde{D}u_k, \quad k \in \mathbb{N}_0^{N-1} \tag{2c}$$

$$\underline{y}_k - s_k^{T_z} \le \tilde{y}_k \le \overline{y}_k + s_k^{T_z}, \quad k \in \mathbb{N}_0^{N-1} \tag{2d}$$

$$\mathbf{0} \le s_k^{T_z}, \quad k \in \mathbb{N}_0^{N-1} \tag{2e}$$

$$u_k = u_{N_c}, \quad k \in \mathbb{N}_{N_c}^{N-1} \tag{2f}$$

$$\underline{u} \le u_k \le \overline{u}, \quad k \in \mathbb{N}_0^{N-1} \tag{2g}$$

$$d_k = d(t + kT_s), \quad k \in \mathbb{N}_0^{N-1} \tag{2h}$$

$$\underline{y}_k = \underline{y}(t + kT_s), \quad k \in \mathbb{N}_0^{N-1} \tag{2i}$$

$$\overline{y}_k = \overline{y}(t + kT_s), \quad k \in \mathbb{N}_0^{N-1} \tag{2j}$$

$$x_0 = \hat{x}(t), \tag{2k}$$

where $\mathbb{N}_0^{N-1} = \{0, 1, \dots, N-1\}$ is a set of integers, $x_k \in \mathbb{R}^{712}$, $u_k \in \mathbb{R}^{21}$, $y_k \in \mathbb{R}^{12}$ and $d_k \in \mathbb{R}^{301}$ represent the values of the states, inputs, outputs and disturbances, respectively, predicted at the kth step of the prediction horizon N and control horizon N_c, respectively. Prediction horizon N defines the length of a time window for which MPC computes the predictions given by the model. Based on the model dynamics we choose N to be equal to one day, i.e. $N = 96$ steps. The control horizon N_c represents the length of a time window for which MPC computes the optimal control actions minimizing the given objective function. Based on simulated model response we choose N_c to be 16 hours, i.e. $N_c = 64$ steps in order to reduce computational time without mitigating the control performance. The predictions are obtained from the LTI prediction model given by Eqs. (2b) and (2c). The $\underline{y}_k$ and $\overline{y}_k$ parameters represent the comfort band given by the constraints (2d), where the variables s_k are used as the slack variables of a comfort band violation. Slack variables are penalized to be non-negative (2e). Computational requirements of the resulting optimization problem are reduced by the so-called move blocking constraint (2f), limiting the number of optimized control actions u_k by control horizon $N_c < N$. The min/max constraints for the control input amplitude are given by (2g). For particular initial conditions (2k), weather forecast (2h) and given comfort bounds (2i) and (2j) the optimization computes the sequence $u_0^*, \dots, u_{N-1}^*$ of control inputs that are optimal with respect to the quadratic objective function (2a) and the constraints. The term $\| \star \|_Q^2$ in the objective function repre-

Table 6
Notation of MPC variables and translation between physical and abstract domain for this case.

Physical domain			Abstract domain						
Variables	Symbol	Description	x	y	m	a	u	d	s
Temperatures [°C]	T	Envelope temperatures	•	–	–	–	–	–	–
	T_z	Zone operative temperatures	–	•	–	–	–	–	–
	$T_{\text{ret}}^{\text{TABS}}$	Water return temperatures TABS	–	–	•	–	–	–	–
	$T_{\text{ret}}^{\text{FH}}$	Water return temperature floor heating	–	–	•	–	–	–	–
	$T_{\text{sup}}^{\text{TABS}}$	Water supply temperatures TABS	–	–	•	–	–	–	–
	$T_{\text{sup}}^{\text{FH}}$	Water supply temperature floor heating	–	–	•	–	–	–	–
	$T_{\text{sup}}^{\text{HP}}$	Water supply temperature heat pump	–	–	•	–	–	–	–
	$T_{\text{sp}}^{\text{HP}}$	Set-point supply temperature heat pump	–	–	–	•	–	–	–
	$T_{\text{sp}}^{\text{TABS}}$	Set-point supply temperature TABS	–	–	–	•	–	–	–
	$T_{\text{sp}}^{\text{FH}}$	Set-point supply temperatures floor heating	–	–	–	•	–	–	–
	$T_{\text{sup}}^{\text{AHU}}$	Air supply temperatures AHU	–	–	–	–	–	•	–
	T_e	Ambient temperature	–	–	–	–	–	•	–
Thermal powers [W]	$\dot{Q}_{\text{TABS}}$	Thermal power of TABS	–	–	–	–	•	–	–
	$\dot{Q}_{\text{FH}}$	Thermal power of floor heating	–	–	–	–	•	–	–
	$\dot{Q}_{\text{rad}}$	Solar radiation	–	–	–	–	–	•	–
	$\dot{Q}_{\text{occ}}$	Occupancy internal gains	–	–	–	–	–	•	–
Component signals	x_{val}	Valve positions TABS [%]	–	–	–	•	–	–	–
	x_{TABS}	ON/OFF signal of TABS pump [{0, 1}]	–	–	–	•	–	–	–
	x_{FH}	ON/OFF signal of FH pump [{0, 1}]	–	–	–	•	–	–	–
	x_{heat}	ON/OFF heating circuit valve [{0, 1}]	–	–	–	•	–	–	–
	x_{cool}	ON/OFF cooling circuit valve [{0, 1}]	–	–	–	•	–	–	–
	x_{HP}	Heat pump mode [{H, AC, PC}]	–	–	–	•	–	–	–
	$x_{\text{TABS,circ}}$	Recirculation of TABS [{0, 1}]	–	–	–	•	–	–	–
Comfort violations [°C]	s^{T_z}	Violations of thermal comfort zones	–	–	–	–	–	–	•
Thermal power violations [W]	$s^{\dot{Q}_{\text{TABS}}}$	Violations of delivered thermal power by TABS	–	–	–	–	–	–	•
	$s^{\dot{Q}_{\text{FH}}}$	Violations of delivered thermal power by FH	–	–	–	–	–	–	•

sents the weighted squared 2-norm, i.e., $\star^T Q \star$, with the weighting matrices Q_s and Q_u given as positive definite diagonal matrices. The first term of the quadratic cost function minimizes the square of the comfort violation, while the second term minimizes the square of the energy use.

3.4. Post-processing of control variables

The computed optimal control inputs $u_0 = [\dot{Q}_{\text{TABS}}, \dot{Q}_{\text{FH}}]$ to be delivered to the building via the receding horizon control (RHC) principle are representing heat flows. However, in a practical setup, we are not able to directly manipulate the heat flows. Instead, we need to map them to the physical actuator variables a optimally. In particular, we control 20 two-way valves of individual circuits of TABS x_{val}, and supply temperature for TABS $T^{\text{TABS}}_{\text{sp}}$ and floor heating $T^{\text{FH}}_{\text{sp}}$, respectively. We compute these values by solving a non-linear optimization problem (NLP) using the heat transfer equation:

$$\min_{x_{\text{val}}, T^{\text{TABS}}_{\text{sp}}, T^{\text{FH}}_{\text{sp}}, s^{\dot{Q}_{\text{TABS}}}, s^{\dot{Q}_{\text{FH}}}} \sum_{i=1}^{n_{\text{TABS}}} x^i_{\text{val}} + ||s^{\dot{Q}_{\text{TABS}}}||^2_{Q_{\text{TABS}}} + ||s^{\dot{Q}_{\text{FH}}}||^2_{Q_{\text{FH}}} \tag{3a}$$

$$\text{s.t. } \dot{Q}_{\text{TABS}} + s^{\dot{Q}_{\text{TABS}}} = x_{\text{val}}\ \dot{m}^{\text{nom}}_{\text{wat,TABS}}\ c_p\ (T^{\text{TABS}}_{\text{sp}} - T^{\text{TABS}}_{\text{ret}}), \tag{3b}$$

$$\dot{Q}_{\text{FH}} + s^{\dot{Q}_{\text{FH}}} = \dot{m}^{\text{nom}}_{\text{wat,FH}}\ c_p\ (T^{\text{FH}}_{\text{sp}} - T^{\text{FH}}_{\text{ret}}), \tag{3c}$$

$$\underline{T}^{\text{TABS}}_{\text{sp}} \le T^{\text{TABS}}_{\text{sp}} \le \overline{T}^{\text{TABS}}_{\text{sp}}, \tag{3d}$$

$$\underline{T}^{\text{FH}}_{\text{sp}} \le T^{\text{FH}}_{\text{sp}} \le \overline{T}^{\text{FH}}_{\text{sp}}, \tag{3e}$$

$$\underline{x}_{\text{val}} \le x_{\text{val}} \le \overline{x}_{\text{val}}. \tag{3f}$$

The objective is to select the supply temperature set-points $T^{\text{TABS}}_{\text{sp}}$, $T^{\text{FH}}_{\text{sp}}$ and valve openings x_{val} for TABS, which minimize the sum of the valve openings, while heavily penalizing the violations of the heat transfer Eqs. (3b) and (3c) via slack variables $s^{\dot{Q}_{\text{TABS}}}$ and $s^{\dot{Q}_{\text{FH}}}$. This formulation, therefore, delivers physically realizable heat flows while minimizing deviations from MPC control actions. Specific heat capacity c_p of the water, together with nominal mass flow rates $\dot{m}_{\text{nom}}$ obtained from the technical sheets of the building are used as constant parameters. The parameters of the problem are the measurements of return temperatures from TABS $T^{\text{TABS}}_{\text{ret}}$ and FH $T^{\text{FH}}_{\text{ret}}$, respectively, supply temperature from heat pump $T^{\text{HP}}_{\text{sup}}$, and computed optimal heat flows $\dot{Q}_{\text{TABS}}$ and $\dot{Q}_{\text{FH}}$. The numerical values of upper and lower bounds for $T^{\text{TABS}}_{\text{sp}}$ and $T^{\text{FH}}_{\text{sp}}$ given by Eqs. (3d) and (3e) are based on the HP modulation mode and supply temperatures obtained from the BMS. The valve modulations x_{val} are bounded based on their corresponding physical constraints (3f).

Besides valves and supply temperatures of TABS and FH, we physically control also supply temperature for HP $T^{\text{HP}}_{\text{sp}}$, HP mode x_{HP}, opening of the distribution circuits via two-way valves for cooling x_{cool} and heating mode x_{heat}, and distribition pumps activation for TABS x_{TABS} and floor heating x_{FH}, respectively. The selection of these variables is defined by heuristic rules described in

Algorithm 1 Post-processing of control variables.

function PostProcess($\dot{Q}_{\text{TABS}}, \dot{Q}_{\text{FH}}, T^{\text{TABS}}_{\text{ret}}, T^{\text{HP}}_{\text{sup}}$)
  if $\sum[\dot{Q}_{\text{TABS}}, \dot{Q}_{\text{FH}}] > 0$ **then** ▷ selection of heating/cooling circuit
    $x_{\text{heat}} = 1$, $x_{\text{cool}} = 0$
  else
    $x_{\text{heat}} = 0$, $x_{\text{cool}} = 1$
  end if
  if $\sum |[\dot{Q}_{\text{TABS}}, \dot{Q}_{\text{FH}}]| < 2e4$ **then** ▷ simultaneous heating and cooling
    $T^{\text{TABS}}_{\text{sp}} = T^{\text{TABS}}_{\text{ret}}$ ▷ $\Delta T^{\text{TABS}} = 0$
    $T^{\text{FH}}_{\text{sp}} = T^{\text{FH}}_{\text{ret}}$ ▷ $\Delta T^{\text{FH}} = 0$
    $x^i_{\text{val}} = 100, \quad i \in \mathbb{N}_1^{n_{\text{TABS}}}$ ▷ valves fully open for recirculation
    $s^{\dot{Q}_{\text{TABS}}} = x_{\text{val}}\ \dot{m}^{\text{nom}}_{\text{wat}}\ c_p\ (T^{\text{TABS}}_{\text{sp}} - T^{\text{TABS}}_{\text{ret}}) - \dot{Q}_{\text{TABS}}$ ▷ update TABS slack variables
    $s^{\dot{Q}_{\text{FH}}} = \dot{m}^{\text{nom}}_{\text{wat}}\ c_p\ (T^{\text{FH}}_{\text{sp}} - T^{\text{FH}}_{\text{ret}}) - \dot{Q}_{\text{FH}}$ ▷ update FH slack variables
    $x_{\text{TABS,circ}} = 1$ ▷ TABS recirculation flag
  else
    Solve NLP (3) to obtain values ofx_{val}, $T^{\text{TABS}}_{\text{sp}}$, $T^{\text{FH}}_{\text{sp}}$, $s^{\dot{Q}_{\text{TABS}}}$, and $s^{\dot{Q}_{\text{FH}}}$.
    $x_{\text{TABS,circ}} = 0$
  end if
  $u_k = [\dot{Q}_{\text{TABS}} + s^{\dot{Q}_{\text{TABS}}}, \dot{Q}_{\text{FH}} + s^{\dot{Q}_{\text{FH}}}]$ ▷ update MPC action for initialization of next computation step
  if $x_{\text{heat}} \vee x_{\text{TABS,circ}}$ **then** ▷ heating circuit
    $x_{\text{HP}} = \text{H}$ ▷ HP heating mode
    if $\sum x_{\text{val}} > 10$ **then** ▷ activation of circulation pumps
      $x_{\text{TABS}} = 1$, $x_{\text{FH}} = 1$
    else
      $x_{\text{TABS}} = 0$, $x_{\text{FH}} = 0$
    end if
    if $x_{\text{TABS,circ}}$ **then** ▷ recirculation mode
      $T^{\text{HP}}_{\text{sp}} = 18$ ▷ HP heating modulation off
    else ▷ heating mode
      $T^{\text{HP}}_{\text{sp}} = T^{\text{TABS}}_{\text{sp}} + 2$ ▷ HP heating modulation on
    end if
  else ▷ cooling circuit
    $x_{\text{HP}} = \text{PC}$ ▷ HP passive cooling mode
    if $\sum x_{\text{val}} > 10$ **then** ▷ activation of circulation pumps
      $x_{\text{TABS}} = 1$, $x_{\text{FH}} = 0$
    else
      $x_{\text{TABS}} = 0$, $x_{\text{FH}} = 0$
    end if
    $T^{\text{HP}}_{\text{sp}} = T^{\text{TABS}}_{\text{sp}} - 2$ ▷ HP cooling modulation on
  end if
end function

Table 7
MPC formulation parameters - modifiers.

Heat flow parameters	Symbol	Description	Associated variables
Specific heat capacity	c_p	Specific heat capacity of water [J kg−1 K−1]	$\dot{Q}_{\text{TABS}}, \dot{Q}_{\text{FH}}$
Nominal mass flow rates	$\dot{m}^{\text{nom}}_{\text{wat}}$	Nominal mass flow rates [ls−1]	$\dot{Q}_{\text{TABS}}, \dot{Q}_{\text{FH}}$

Auxiliary parameters	Symbol	Description	Associated variables
Weighting factor	$Q_\star$	Weighting for the particular term in the objective function	$s^{T_z}, u, s^{\dot{Q}_{\text{TABS}}}, s^{\dot{Q}_{\text{FH}}}$
Sampling time	T_s	Time-step used in the optimization problem	all
Dimensionality quantifier	$n_\star$	Cardinality of the vector elements	all

Algorithm 1. First step is the selection of heating or cooling circuit of TABS and FH (lines 2 to 6) based on optimal heat flows $[\dot{Q}_{\text{TABS}}, \dot{Q}_{\text{FH}}] = u_0$ by solving MPC problem (2). In the special case of simultaneous heating and cooling with small heat imbalance (lines 7 to 13) we open all valves in TABS and FH circuits to recirculate the water with $\Delta T = 0$. This is a straightforward and energy efficient strategy for balancing the temperatures within the building by exchanging the heat from overheated zones to heat-demanding zones. This situation happens mostly during the transition period when few zones may require heating and other cooling to keep their temperatures within prescribed comfort bounds. In the standard cases (lines 14 to 17) of solely heating or cooling we solve NLP (3). In either case, optimal control actions computed by MPC (2) are corrected for the next computational step by the amount of missing heat captured by slack variables $s^{\dot{Q}_{\text{TABS}}}$ and $s^{\dot{Q}_{\text{FH}}}$ (line 18). In heating mode (lines 19 to 30), the HP mode is set to heating (line 20), the circulation pumps are activated for both TABS and FH based on the opening of the circuit valves (lines 21 to 25). If we are in TABS recirculation mode activated by simulaneous heating and cooling $x_{\text{TABS,circ}} = 1$, the supply temperature of the HP is set to 18°C, which corresponds to zero voltage to the heat pump (lines 26 to 27). Otherwise, we modulate the HP supply temperature to be above the set-point for TABS supply temperature (lines 28 to 30). Similar rules apply for the cooling circuit as well (lines 31 to 39). The HP mode is set to passive cooling (line 32). Based on valve openings the program activates the circulation pump only for TABS (lines 33 to 37). The supply temperature of the HP is set to be lower than the set-point for TABS supply temperature (line 38).

4. Communication and operational infrastructure

This section describes individual components and the overall architecture of the communication infrastructure, which is necessary for the successful implementation of advanced optimal control strategies in real buildings.

4.1. Cloud-based SCADA system

The Hollandsch Huys building is governed by a Priva Building Management System (BMS) installed on a local computer in the building's basement. The Priva BMS allows plotting and manual change of selected variables, but does not provide a communication interface necessary for MPC. Unfortunately, the world of building automation is still far from standardization of communication protocols and data formats. Therefore we had to solve the problem of integrating the BMS running on site and the MPC server running remotely. We decided to use cloud-based Mervis SCADA [31] and it's ecosystem of applications to solve this task. We installed a parallel communication system interacting with the Priva controller via Modbus TCP protocol. All available Modbus variables are copied into the Mervis RTWindows service which communicates current values into the Mervis Proxy cloud server and also stores all values periodically into the Mervis DB server. Mervis SCADA then offers a set of APIs to read online values, write new values back to the BMS, or download the historical data. Usually, data from the BMS are not secured, and there is no support for encryption on BMS or PLC level. In our case security is achieved by encryption (HTTPS) via Mervis.

The motivating factor behind the cloud-based architecture is its compatibility with a commercially appealing control as a service concept, in our case, supported by Mervis.[3] The advantages of cloud-based solutions are user-friendly and easy access to the real-time building data from any place via a secured web-based application, automatic data back-ups, reliability and customer support, and no need for additional hardware investments. The disadvantage is the need for an internet connection, which may represent a single point of failure. This downside was mitigated by implementing a watchdog procedure with a back-up RBC taking over the control of the building in case of communication shutdowns. An advanced solution would be the replacement of the back-up RBC with a machine learning-based controller trained by mimicking the MPC as proposed in [32].

4.2. Modbus communication

In Hollandsch Huys we communicate 165 data points in real-time via Modbus. The 96 reading variables consist of 28 zone temperatures, 18 concrete core temperatures, 23 TABS and FH return temperatures, 2 supply temperatures for TABS and FH, 2 supply temperatures for AHUs, 6 measurements for supply and return temperatures of the HP in different operational modes, 5 discrete variables indicating the operation of the HP, 2 variables for inlet and outlet temperatures of the borefield, and 10 auxiliary variables with mixed nature. The 69 writing variables represent 21 valve modulations for TABS, 2 valves for switching between cooling and heating circuit of TABS, 2 circulation pumps for TABS and FH, 2 temperature setpoints for TABS and FH, 3 discrete modes for the HP, 2 temperature setpoints for HP in heating and cooling mode, 2 temperature setpoints for AHUs, 1 watchdog flag, and 34 auxiliary variables representing computed optimal heat flows, comfort bounds, and a subset of weather forecast variables. All Modbus data from the Hollandsch Huysh building is available in Mervis SCADA.

4.3. Design and operation

Fig. 8 demonstrates the overall technical scheme for design and operation phase of MPC in a real office building.

The design phase starts with studying the technical sheets and continues with a visit to the building to get acquainted with the building's HVAC and BMS system. Based on a detailed technical description of the building systems a white-box model is developed and linearized as described in Section 2. Dark Sky weather forecast service is used for real-time data acquisition via python Dark Sky API [28], generating a text file in a TMY format, which is subsequently used for initialization of the non-linear model wrapped into FMU and simulated in Simulink environment to obtain the disturbance forecast for MPC as elaborated in Section 2.5. The linearized model is used for the Kalman Filter and MPC design via

[3] https://mervis.info.

Table 8
MPC formulation parameters - bounds.

Bounds	Symbol	Description	Associated variables	Abstract domain
Comfort bounds [°C]	$\underline{T}_z$, $\overline{T}_z$	Lower/upper bounds of thermal comfort zones	T_z	$r = \{\underline{y}, \overline{y}\}$
Thermal power limits [W]	$\underline{\dot{Q}}_{\text{TABS}}$, $\overline{\dot{Q}}_{\text{TABS}}$, $\underline{\dot{Q}}_{\text{FH}}$, $\overline{\dot{Q}}_{\text{FH}}$	Min/max thermal powers	Q_{TABS}, Q_{FH}	$\underline{u}$, $\overline{u}$
Supply temperature bounds [°C]	$\underline{T}^{\text{TABS}}_{\text{sp}}$, $\overline{T}^{\text{TABS}}_{\text{sp}}$ $\underline{T}^{\text{FH}}_{\text{sp}}$, $\overline{T}^{\text{FH}}_{\text{sp}}$	Lower/upper bounds HVAC supply temperatures	$T^{\text{TABS}}_{\text{sp}}$, $T^{\text{FH}}_{\text{sp}}$	–
Valve position limits [%]	$\underline{x}_{\text{val}}$, $\overline{x}_{\text{val}}$	Min/max valves position	x_{val}	–

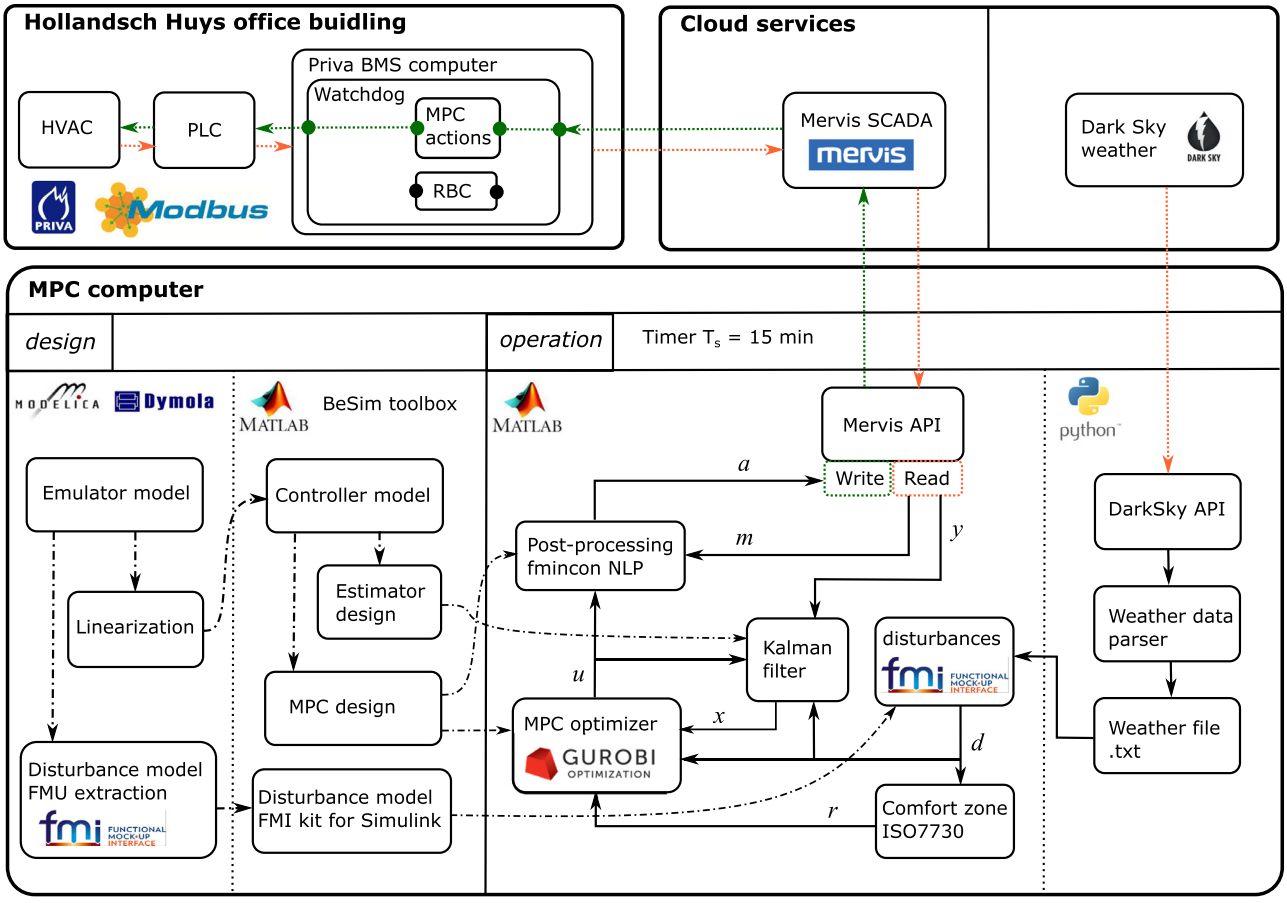

Fig. 8. Overall technical scheme for design and operation of MPC in Hollandsch Huys office building.

the BeSim toolbox in Matlab [33]. BeSim is built upon the modelling and optimization toolbox YALMIP [34]. MPC problem (2) is cast as a QP problem for the solution of which the state of the art optimization solver GUROBI [35] is used. Matlab's built-in solver `fmincon` is used for the solution of the post-processing NLP (3). Simulations with full-year historical data are performed to test and tune the formulation and computational aspects of the developed control strategy (Section 3). For real operation, a remote desktop connection to the building's BMS computer is necessary due to software changes in the original BMS system. As a final step, real-time remote communication via Modbus is established using Mervis, a cloud-based SCADA system, with Mervis Matlab API used for reading and writing of Modbus variables, as described in previous sections.

The operational phase is executed via MATLAB timer with a sampling period of 15 min. The procedures within each step are conceptually summarized in Algorithm 2.

All measurements are obtained from the past 15 min of operation with 60sec sampling interval, hence each data point is represented by 1 to 15 measurements, which are averaged to a single value. This approach is chosen to filter out measurement errors and missing values caused by communication drops. All procedures in Algorithm 2 are executed within the try and catch statements, which, in case of error, recover the numerical values from the previous execution step. In case of communication drops between the BMS computer and the cloud services, the local watchdog starts a countdown of 60min after which the operation reverts to the RBC strategy. An email notification with an alarm message is generated each time the fallback strategy is triggered. This ensures an automated error handling and keeps the system running 24/7 regardless of computational or communication errors. A single runtime of the Algorithm 2 takes approximately 50sec on average, of which 25sec are used for disturbance forecast via the FMU model, 20sec for communication, and 5sec for solving optimization problems.

Table 4
Dimensions of the linear building envelope model.

Notation	Description	Values
n_x	number of states	700
n_u	number of inputs	21
n_y	number of outputs	12
n_r	number of comfort bounds	24
n_d	number of forecasted disturbances	301

5. Experimental results

This section verifies the feasibility of the proposed cloud-based implementation methodology and evaluates the field test performance of the white-box MPC in the Hollandsch Huys office building. The experiment was conducted from 18th of April until 23th of September 2019. However, uneven distribution of the ambient temperature during the operation of MPC and RBC casts their direct comparison a difficult task. For the sake of increased fairness, we evaluate the performance on a subset of the gathered data with a similar distribution of the weather conditions for both control strategies. In this case, it corresponds to the transient seasons with daily mean ambient temperatures falling in the range 13°C-25°C. We also exclude the one day after the switch between the control strategies, to mitigate their cross-influence. The resulting

Algorithm 2 Real-time MPC timer procedure.

function RealTimeMPC(MPC (2), NLP (3), Mervis SCADA)
  try ▷ outputs measurements
    Read measurements of $y(t)$ over past 15 min via Mervis SCADA API.
    Remove error values and missing entries in $y(t)$.
  catch Error in reading $y(t)$
    Use $y(t-1)$ from previous execution step.
  end try
  try ▷ disturbances forecast
    Load the TMY file generated from DarkSky API and simulate FMU non-linear building model to obtain disturbances $d(t,\dots,t+N-1)$.
    Obtain schedules of $T_{\text{sup}}^{\text{AHU}}$ and append their forecast to $d(t,\dots,t+N-1)$.
  catch Error in computing $d(t,\dots,t+N-1)$
    Use disturbance forecast from previous execution step forward-shifted with one step ahead.
  end try
  try ▷ comfort zone forecast
    Generate comfort bound forecast $r(t,\dots,t+N-1)$.
  catch Error in computing $r(t,\dots,t+N-1)$
    Use comfort bound forecast from previous execution step forward-shifted with one step ahead.
  end try
  try ▷ state estimation and MPC
    Compute state estimates $x(t)$ by running Kalman Filter with 20 iterations using current measured outputs $y(t)$ and optimal control actions $u(t-1)$ from previous executions step.
    Solve MPC optimization problem (2) to compute u_0.
  catch Error in computing u_0
    Reuse $u_0(t-1)$ from previous execution step.
  end try
  try ▷ HVAC measurements
    Obtain measurements of $T_{\text{ret}}^{\text{TABS}}$, and $T_{\text{sup}}^{\text{HP}}$.
    Remove error values and missing entries in $T_{\text{ret}}^{\text{TABS}}$, and $T_{\text{sup}}^{\text{HP}}$.
  catch Error in reading $T_{\text{ret}}^{\text{TABS}}$, and $T_{\text{sup}}^{\text{HP}}$
    Reuse the values of $T_{\text{ret}}^{\text{TABS}}$, and $T_{\text{sup}}^{\text{HP}}$ from previous execution step.
  end try
  try ▷ HVAC actuators
    Execute post-processing Algorithm 1 to compute the values of actuator variables $a(t)$.
  catch Error in post-processing the actuators $a(t)$
    Reuse the values of $a(t-1)$ from previous execution step.
  end try
  if watchdogFlag $= 0$ **then** ▷ watchdog
    watchdogFlag $= 1$
  else
    watchdogFlag $= 0$
  end if
  try ▷ write to BMS
    Write computed actuator variables $T_{\text{sp}}^{\text{HP}}$, $T_{\text{sp}}^{\text{TABS}}$, $T_{\text{sp}}^{\text{FH}}$, x_{val}, x_{TABS}, x_{FH}, x_{cool}, x_{heat}, x_{HP}, watchdogFlag to Modbus via Mervis SCADA API.
  catch Error in writing computed values to Modbus.
    Generate error message.
  end try
end function

dataset now consists of 79 days (35 for MPC, 44 for RBC) with mean ambient temperatures equal to 16.8°C and 18.0°C for MPC and RBC datasets, respectively. From the control perspective, the transient seasons are particularly challenging because some zones need heating and other cooling to satisfy the thermal comfort requirements.

5.1. Performance comparison of MPC with RBC

The energy savings attributed to MPC operation during the transient season are emphasized in Fig. 9. The left figure displays the daily HP energy use as a function of the average daily ambient temperature. The middle figure in Fig. 9 shows a subset of days with cooling demand represented via the daily HP energy use as a function of the cooling degree days (CDD). The right figure in Fig. 9 captures a subset of days with heating demand via the daily HP energy use as a function of the heating the degree days (HDD). CDD and HDD are defined as the number of degrees that a daily average temperature is above or below 18°C, respectively. By differentiating MPC and RBC operational days, we can identify correlated linear relations between energy use and ambient temperature, CDD, and HDD, respectively. The visual analysis of Fig. 9 reveals substantial improvements in favor of MPC.

Fig. 10, on the other hand, captures the comfort performance of MPC and RBC given as the average thermal discomfort per zone per day given as a function of the daily HP energy use. The black dashed line represents a comfort threshold equal to 0.275Kh per zone per day (100Kh per year), similarly as used in [36], and represents a violation level as it would be tolerated according to the standards [37,38]. The left figure represents the whole dataset, while the middle and right figure stands for days with a cooling and heating demand, respectively. Besides lower energy demand, MPC has also a lower discomfort rate on average compared to RBC. Satisfaction of the thermal constraints on the evaluated dataset has been particularly challenging for warm days with high cooling demand. The corresponding HP energy savings on the datasets with similar mean ambient temperatures are equal to 53.5%, with a thermal comfort improvement equal to 36.9%. The comparison of MPC and RBC performance is compactly summarized in Table 9.

However, it is essential to mention that these improvements are preliminary, attributed to the transient seasons only and can not be generalized to yearly performance across all seasons with a high degree of confidence. Nevertheless, these results are promising and encouraging towards a further assessment of MPC performance in the long-term.

5.2. Details of MPC and RBC operation

The differences between the MPC and RBC operation are investigated into more details on two similar weeks with cooling demand. Fig. 11 shows the corresponding time-series profiles for both control strategies. The six upper figures demonstrate the evolution of zone temperatures with similar initial conditions. The seventh and eighth figure, capture the supply and return temperatures of TABS as an indicator of the heat flows delivered to the building. The bottom figures confirm that both weeks have similar ambient temperature profiles. Fig. 11 demonstrates that the MPC operation differs significantly from RBC. The first difference is in the satisfaction of comfort constraints. In contrast to the RBC, the MPC is explicitly aware of the prescribed comfort zone and predicted indoor temperatures, which results in anticipatory behavior, minimizing day-ahead discomfort and energy use. The RBC, on the other hand, completely lacks the feedback from the zone temperature measurements and is thus unable to react on actual conditions within the building.

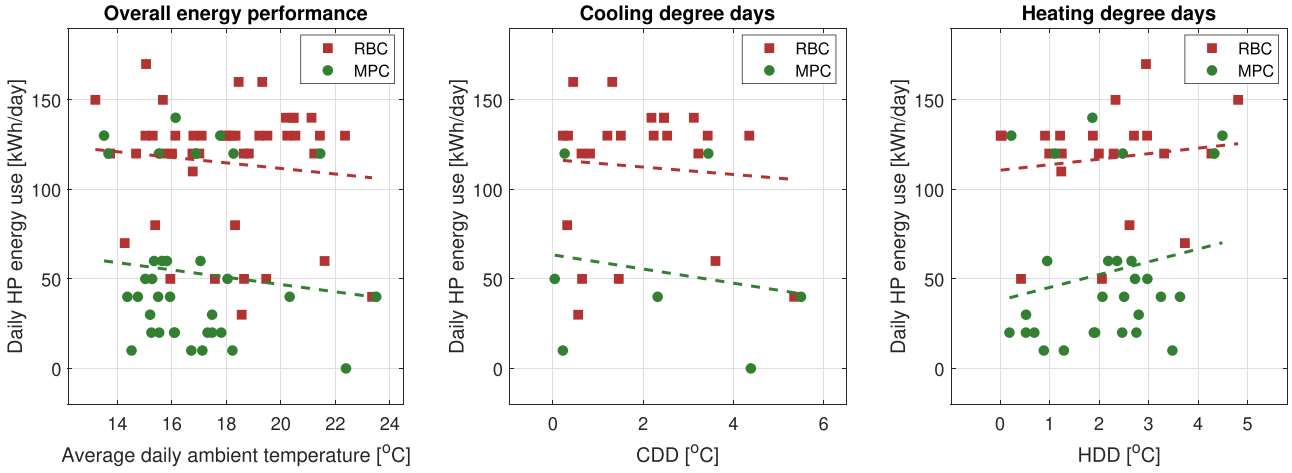

Fig. 9. The energy performance of MPC and RBC during the transient seasons. The daily heat pump energy use is displayed as a function of the average daily ambient temperature, cooling degree days (CDD), and heating degree days (HDD), respectively.

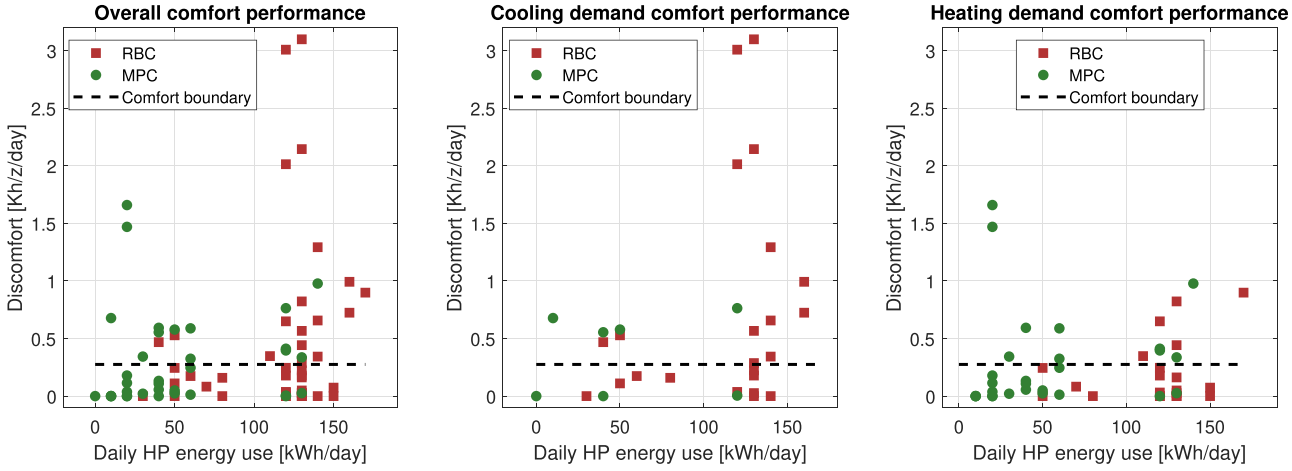

Fig. 10. The comfort performance of MPC and RBC during the transient seasons. The daily average thermal discomfort per zone id displayed as a function of the daily HP energy use.

Table 9
Comparison of MPC and RBC operational performance during the transient seasons.

Quantitative Objectives	Key Performance Indicators (KPIs)	Units	MPC Operation	RBC Operation
Energy performance	Mean HP energy use per day	kWh	53.4	114.8
	Energy savings	%	53.5	–
Thermal comfort	Mean discomfort per zone per day	Kh/z/day	0.31	0.48
	Comfort improvement	%	36.9	–
Conditions	Average ambient temperature	°C	16.8	18.0
Dataset	Number of evaluated days	–	35	44

The RBC makes its decisions solely based on the fixed rules and the heating/cooling curve driven by a three day average of the ambient temperature as described in Section 2.3. As a consequence, RBC exhibits delayed reactive behavior w.r.t. the weather conditions and a rigid control behavior of the TABS. Middle figure in Fig. 11a displays almost constant ΔT between the supply and return temperature of TABS controlled by RBC. Three bumps with higher supply temperatures represent the delayed response of the RBC on three colder nights at the beginning of the week. During these periods the 3-day mean ambient temperature was below 12°C, and the RBC switched from the cooling mode to the heating mode. Moreover, due to the rigid modulation of the TABS distribution circuits valves, RBC is not capable of leveraging the full potential of the TABS mass flow rates. Because of the fixed schedules of the valve opening for the duration of 10min per circuit per hour, the RBC consistently uses roughly 17% of the TABS full capacity. Additionally, the RBC is not programmed to recirculate the water in TABS without interaction with the HP.

MPC, on the other hand, is capable of commanding the water recirculation in TABS without the use of the HP, resulting in substantial energy savings. TABS recirculation is a very efficient way of balancing the zone temperatures via transferring the heat from warmer to colder zones, a feature particularly useful during the transient seasons when both heating and cooling demand are often required at the same time in different parts of the building. Furthermore, the MPC exhibits anticipatory behavior w.r.t. the weather conditions and comfort bounds and dynamically modulates the mass flows and ΔT of the TABS as well as the operational mode of the HP. These capabilities are visible in the middle figure of Fig. 11b depicting the supply and return temperatures of TABS

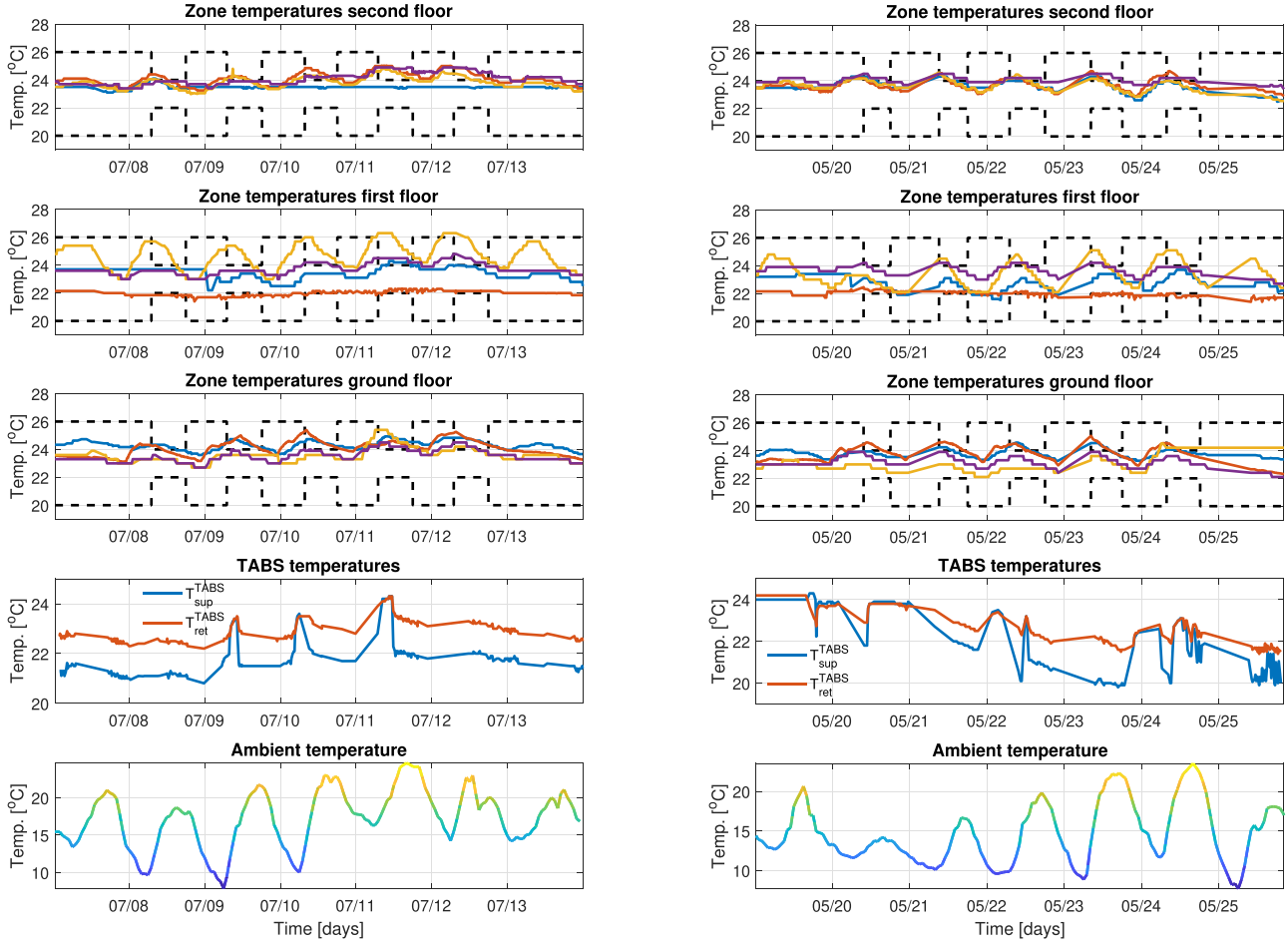

(a) RBC. *(b) MPC.*

Fig. 11. Comparison of RBC and MPC building operation on two similar weeks with cooling demand.

controlled by MPC. Based on the forecast of relatively lower ambient temperature for 21st and 22th of May, MPC decides to recirculate the water in TABS for most of the time, resulting in a ΔT close to 0°C. Different behavior is executed with the forecast of warmer days for 23rd and 24th of May. MPC here activates passive cooling for most of the time and increases ΔT such that the building is pre-cooled to satisfy the thermal constraints. The bottom part of Fig. 11b also shows that despite the accurate predictive capabilities, the MPC does not fully satisfy the comfort bounds. This is the consequence of the interplay of multiple factors such as uncertainties in the weather and occupancy forecasts, the control input offsets caused by the low-level controllers, and the plant-model mismatch. It is also important to emphasize the challenge of keeping the zone temperatures in a narrow range of 22 °C–24 °C during the weekdays with significant influence of mainly internal and partially solar gains only by controlling slow-reacting TABS and FH. Even though, compared to RBC, MPC is capable of decreasing the variance of zone temperature profiles and minimizes the overall constraints violations. A secondary fast reacting system (controlled by MPC) and the availability of active cooling will help in guaranteeing thermal comfort, leading to the MPC hybridgeotabs concept [39].

6. Conclusions

This paper reports a successful cloud-based implementation and remote operation of white-box model predictive control (MPC) in a hybridGEOTABS office building. We introduce a detailed implementation methodology consisting of three interconnected parts: building modeling, control configuration, and communication and SCADA system architecture. The high-fidelity building model is developed using the Modelica language. The localized weather forecast is computed via simulating the non-linear model initialized with the weather forecast obtained from the DarkSky web-service. MPC and Kalman filter are designed and run in the Matlab environment. MPC computes optimal heat flows, which are subsequently post-processed into low-level actuator signals by solving a non-linear optimization problem. The overall control system runs on a remote desktop computer and securely communicates with the building's BMS via the cloud-based SCADA system Mervis using the Modbus protocol and HTTPS encoding. The computational efficiency of the underlying optimization is achieved by decoupling the non-linearities into separate sub-problems. As a result, the whole execution procedure takes less than 1 min to run. Taking into account the 15min sampling period, the reported implementation leaves plenty of space for potential execution of the error handling procedures or system restarts in case of communication dropouts.

Real operation evaluated during the transient seasons demonstrates preliminary savings of the heat pump energy use equal to 53.5%. On top of that MPC improved thermal comfort by 36.9% by keeping the zone temperatures closer to the prescribed comfort bounds. This pilot implementation and real operation of white-box MPC demonstrates the feasibility, computational efficiency, and

preliminary performance gains w.r.t. the classical RBC strategy. It is essential to mention that these results are obtained from the evaluation of the operation during the transient seasons and hence can not be generalized to the full-year performance across various seasons. However, the reported results are nevertheless auspicious for further development, and cast a light into the energy savings and comfort improvement potential of the high fidelity MPC for office buildings.

Future work includes the full-year performance evaluation, modeling and mitigation of the uncertainties in weather and occupancy forecast via stochastic MPC, modeling and compensating of the control input errors caused by the low-level P controllers. From the practical perspective of the reduction of the deployment cost and increased operational robustness of a cloud-based solution, the authors plan to enhance the implementation methodology with the local deployment of deep neural network control policies trained on the MPC operational data.

Declaration of Competing Interest

The authors whose names are listed immediately below certify that they have NO affiliations with or involvement in any organization or entity with any financial interest (such as honoraria; educational grants; participation in speakers' bureaus; membership, employment, consultancies, stock ownership, or other equity interest; and expert testimony or patent-licensing arrangements), or non-financial interest (such as personal or professional relationships, affiliations, knowledge or beliefs) in the subject matter or materials discussed in this manuscript.

CRediT authorship contribution statement

Ján Drgoňa: Conceptualization, Methodology, Software, Investigation, Data curation, Formal analysis, Visualization, Writing - original draft. **Damien Picard:** Methodology, Software, Writing - review & editing. **Lieve Helsen:** Methodology, Funding acquisition, Resources, Project administration, Supervision, Writing - review & editing.

Acknowledgement

The authors would like to thank the building owners of Hollandsch Huys, namely Veronique Houben and Ignace Houben for their open attitude and willingness to provide access to the building for research purposes. The programming contribution of Filip Dhondt and Martin Chlupac towards enabling Modbus communication with building management system is acknowledged.

The authors also acknowledge the financial support of the European Union via the EU-H2020-GEOTECH project 'Geothermal Technology for Economic Cooling and Heating'. The authors also acknowledge the financial support by IWT and WTCB in the frame of the IWT-VIS Traject SMART GEOTHERM focusing on the integration of thermal energy storage and thermal inertia in geothermal concepts for smart heating and cooling of (medium) large buildings.

This work emerged from the IBPSA Project 1, an international project conducted under the umbrella of the International Building Performance Simulation Association (IBPSA). Project 1 will develop and demonstrate a BIM/GIS and Modelica Framework for building and community energy system design and operation.

References

[1] IIE International Energy Agency for Energy Efficiency Cooperation, Building Energy Performance Metrics - Supporting Energy Efficiency Progress in Major Economies, Technical Report, IEA Publications, 2015.
[2] EU policy: Revised Energy Performance of Buildings Directive (EPBD), EUR-Lex - 32018L0844 - EN, Technical Report, European Parliament, 2018.
[3] C. Aghemo, J. Virgone, G.V. Fracastoro, A. Pellegrino, L. Blaso, J. Savoyat, K. Johannes, Management and monitoring of public buildings through ICT based systems: Control rules for energy saving with lighting and HVAC services, Front. Archit. Res. 2 (2) (2013) 147–161.
[4] M. Sourbron, C. Verhelst, L. Helsen, Building models for model predictive control of office buildings with concrete core activation, J. Build. Perform. Simul. 6 (3) (2013) 175–198, doi:10.1080/19401493.2012.680497.
[5] D. Gyalistras, M. Gwerder, F. Schildbach, C. Jones, M. Morari, B. Lehmann, K. Wirth, V. Stauch, Analysis of Energy Savings Potentials for Integrated Room Automation, Clima - RHEVA World Congress, Antalya, Turkey, 2010.
[6] M.d. M. Castilla, J.D. Álvarez, F.d. A. Rodriguez, M. Berenguel, Comfort Control in Buildings, Springer-Verlag London. 10.1007/978-1-4471-6347-3.
[7] J. Širokỳ, F. Oldewurtel, J. Cigler, S. Prívara, Experimental analysis of model predictive control for an energy efficient building heating system, Appl. Energy 88 (9) (2011) 3079–3087.
[8] F. Jorissen, Toolchain for Optimal Control and Design of Energy Systems in Buildings, 2018 PhD Thesis.
[9] D. Picard, Modeling, Optimal Control and HVAC Design of Large Buildings using Ground Source Heat Pump Systems, 2017 PhD Thesis.
[10] J. Cigler, D. Gyalistras, J. irok℃, V. Tiet, L. Ferkl, Beyond theory: the challenge of implementing model predictive control in buildings, in: Proceedings of 11th Rehva World Congress, Clima, 2013.
[11] E. Žáčeková, Z. Váňa, J. Cigler, Towards the real-life implementation of MPC for an office building: identification issues, Appl. Energy 135 (2014) 53–62.
[12] S. Prívara, J. Široký, L. Ferkl, J. Cigler, Model predictive control of a building heating system: the first experience, Energy Build. 43 (2–3) (2011) 564–572.
[13] Y. Ma, F. Borrelli, B. Hencey, B. Coffey, S. Bengea, P. Haves, Model predictive control for the operation of building cooling systems, Control Syst. Technol. IEEE Trans. 20 (3) (2012) 796–803.
[14] J. Ma, S.J. Qin, T. Salsbury, Application of economic MPC to the energy and demand minimization of a commercial building, J. Process Control 24 (8) (2014) 1282–1291, doi:10.1016/j.jprocont.2014.06.011.
[15] H.B. Gunay, J. Bursill, B. Huchuk, W. O'Brien, I. Beausoleil-Morrison, Shortest-prediction-horizon model-based predictive control for individual offices, Build. Environ. 82 (2014) 408–419, doi:10.1016/j.buildenv.2014.09.011.
[16] R.D. Coninck, L. Helsen, Practical implementation and evaluation of model predictive control for an office building in Brussels, Energy Build. 111 (2016) 290–298, doi:10.1016/j.enbuild.2015.11.014.
[17] T. Hilliard, L. Swan, Z. Qin, Experimental implementation of whole building mpc with zone based thermal comfort adjustments, Build. Environ. 125 (2017) 326–338, doi:10.1016/j.buildenv.2017.09.003.
[18] F. Jorissen, D. Picard, I. Cupeiro Figueroa, W. Boydens, L. Helsen, Towards real MPC implementation in an office building using TACO, in: 5th International High Performance Buildings Conference at Purdue, West Lafayette, IN, USA, 2018.
[19] M. Ogawa, H. Endo, H. Fukuda, H. Kodama, T. Sugimoto, T. Horie, T. Maruyama, M. Kondo, Cooling control based on model predictive control using temperature information of it equipment for modular data center utilizing fresh-air, in: 2013 13th International Conference on Control, Automation and Systems (ICCAS 2013), 2013, pp. 1815–1820, doi:10.1109/ICCAS.2013.6704235.
[20] N. Lazic, T. Lu, C. Boutilier, M. Ryu, E.J. Wong, B. Roy, G. Imwalle, Data center cooling using model-predictive control, in: Proceedings of the Thirty-second Conference on Neural Information Processing Systems (NeurIPS-18), Montreal, QC, 2018, pp. 3818–3827.
[21] Z. áňa, J. Cigler, J. Široký, E. Žáčeková, L. Ferkl, Model-based energy efficient control applied to an office building, Journal of Process Control 24 (6) (2014) 790–797. Energy Efficient Buildings Special Issue. doi: 10.1016/j.jprocont.2014.01.016.
[22] D. Picard, M. Sourbron, F. Jorissen, J. Cigler, L. Ferkl, L. Helsen, Comparison of model predictive control performance using grey-box and white-box controller models, in: Proceedings of the 4th International High Performance Buildings Conference, West-Lafayette, Indiana, USA, 2016, pp. 1–10.
[23] D. Picard, J. Drgoňa, M. Kvasnica, L. Helsen, Impact of the controller model complexity on model predictive control performance for buildings, Energy Build. 152 (2017) 739–751, doi:10.1016/j.enbuild.2017.07.027.
[24] E. Záceková, Z. Vána, J. Hoogmartens, C. Verhelst, M. Sourbron, L. Ferkl, L. Helsen, Identification for model based predictive control applied to an office building with a thermally activated building systems, VDI-Society fõr Civil Engineering and Building Services; Dõsseldorf, Teloy, Tanja, 2013, pp. 2430–2439.
[25] R. Baetens, R. De Coninck, F. Jorissen, D. Picard, L. Helsen, D. Saelens, OpenIDEAS - an open framework for integrated district energy simulations, in: Proceedings of Building Simulation 2015, Hyderabad, India, 2015.
[26] D. Picard, F. Jorissen, L. Helsen, Methodology for obtaining linear state space building energy simulation models, in: Proceedings of the 11th International Modelica Conference, Paris, France, 2015, pp. 51–58.
[27] W. Parys, D. Saelens, H. Hens, Coupling of dynamic building simulation with stochastic modelling of occupant behaviour in offices–a review-based integrated methodology, J. Build. Perform. Simul. 4 (4) (2011) 339–358.
[28] L. The Dark Sky Company, Dark Sky API.
[29] K. Muske, T.A. Badgwell, Disturbance modeling for offset-free linear model predictive control, J. Process Control 12 (5) (2002) 617–632.

[30] J. Drgoňa, M. Klaučo, M. Kvasnica, MPC-based reference governors for thermostatically controlled residential buildings, in: 2015 54th IEEE Conference on Decision and Control (CDC), 2015, pp. 1334–1339, doi:10.1109/CDC.2015.7402396.
[31] Mervis, Mervis SCADA. Consulted on May 2019., (https://kb.mervis.info/doku.php/en:mervis-scada:00-start).
[32] J. Drgoňa, D. Picard, M. Kvasnica, L. Helsen, Approximate model predictive building control via machine learning, Appl. Energy 218 (2018) 199–216, doi:10.1016/j.apenergy.2018.02.156.
[33] J. Drgoňa, BeSim Toolbox: Fast Development, and Simulation of Advanced Building Control, 2019, https://github.com/drgona/BeSim.
[34] J. Löfberg, YALMIP : a toolbox for modeling and optimization in MATLAB, in: Proc. of the CACSD Conference, Taipei, Taiwan, 2004. Available from http://users.isy.liu.se/johanl/yalmip/.
[35] I. Gurobi Optimization, Gurobi optimizer reference manual, 2012.
[36] F. Oldewurtel, A. Parisio, C. Jones, D. Gyalistras, M. Gwerder, V. Stauch, B. Lehmann, M. Morari, Use of model predictive control and weather forecasts for energy efficient building climate control, Energy Build. 45 (2012) 15–27.
[37] C. Comite'Europe'en de Normalisation, Indoor environmental input parameters for design and assessment of energy performance of buildings addressing indoor air quality, thermal environment, lighting and acoustics, EN 15251 (2007).
[38] I.O. for Standardization, ISO 7730 2005-11-15 Ergonomics of the Thermal Environment: Analytical Determination and Interpretation of Thermal Comfort Using Calculation of the PMV and PPD Indices and Local Thermal Comfort Criteria, International standards, ISO, 2005.
[39] E. Himpe, M. Vercautere, W. Boydens, L. Helsen, J. Laverge, GEOTABS concept and design : state-of-the-art, challenges and solutions, in: Proceedings of the REHVA Annual Meeting Conference Low Carbon Technologies in HVAC, Brussels„ 2018, p. 8.